Article

Effect of Molecular Weight on the Exponential Growth and Morphology of Hyaluronan/Chitosan Multilayers: A Surface Plasmon Resonance Spectroscopy and Atomic Force Microscopy Investigation

Piotr Kujawa, Patricia Moraille, Jacqueline Sanchez, Antonella Badia, and Franoise M. Winnik

J. Am. Chem. Soc., **2005**, 127 (25), 9224-9234• DOI: 10.1021/ja044385n • Publication Date (Web): 04 June 2005

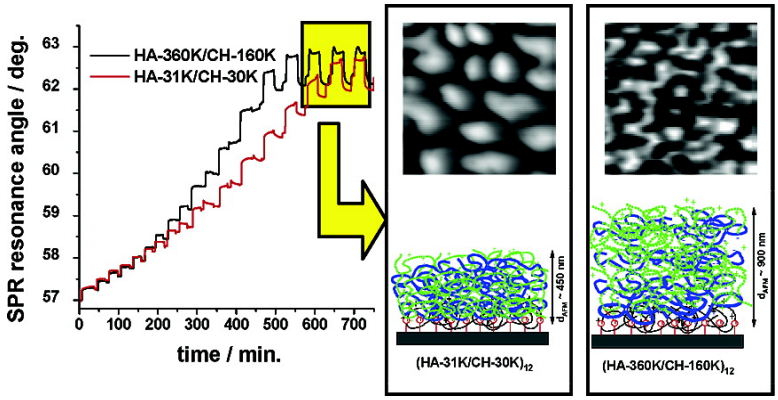

More About This Article

Additional resources and features associated with this article are available within the HTML version:

- Supporting Information
- Links to the 19 articles that cite this article, as of the time of this article download
- Access to high resolution figures
- Links to articles and content related to this article
- Copyright permission to reproduce figures and/or text from this article

View the Full Text HTML

J|A|C|S
ARTICLES
Published on Web 06/04/2005

Effect of Molecular Weight on the Exponential Growth and Morphology of Hyaluronan/Chitosan Multilayers: A Surface Plasmon Resonance Spectroscopy and Atomic Force Microscopy Investigation

Piotr Kujawa,[†] Patricia Moraille,[‡] Jacqueline Sanchez,[‡] Antonella Badia,*[,‡,§] and Françoise M. Winnik*[,†,‡,§]

Contribution from the Faculté de Pharmacie, Département de Chimie, and Center for Self-Assembled Chemical Structures, Université de Montréal, C. P. 6128, Succursale Centre-Ville, Montréal QC, Canada H3C 3J7

Received September 15, 2004; E-mail: francoise.winnik@umontreal.ca; antonella.badia@umontreal.ca

Abstract: The layer-by-layer growth of multilayer assemblies of two polysaccharides, the polyanion hyaluronan (HA) and the polycation chitosan (CH), was investigated using atomic force microscopy (AFM) and surface plasmon resonance (SPR) spectroscopy, with primary emphasis on the effect of the polysaccharide molecular weights on the film thickness and surface morphology. The HA/CH multilayers exhibit an exponential increase of the optical film thickness with the number of deposited bilayers. We show that the multilayer thickness at a given stage depends on the size of both CH, the diffusing polyelectrolyte, and HA, the nondiffusing species. Assemblies (12 bilayers) of high molecular weight polysaccharides (HA, 360 000; CH, 160 000) were twice as thick (~900 nm vs ~450 nm) as those obtained with low molecular weight polymers (HA, 30 000; CH, 31 000), as assessed by AFM scratch tests. The exponential growth rate is the same for the high and low molecular weight pairs; the larger film thicknesses observed by SPR and by AFM arising from *an earlier onset* of the steep exponential growth phase in the case of the high molecular weight pair. In all cases, isolated islets form during the deposition of the first CH layer onto the underlying HA. Upon further film growth, individual islets coalesce into larger vermiculate features. The transition from distinct islands to vermiculate structures depends on the molecular weights of the polysaccharides and the lower molecular weight construct presents larger wormlike surface domains than the high molecular weight pair.

Introduction

The adsorption of polyelectrolytes onto surfaces is a phenomenon that has attracted the interest of polymer scientists for several decades, not only from a theoretical stand point,[1] but also from the point of view of its numerous technologically important applications.[2] Of particular note in this area is the emergence of the technique of layer-by-layer (LbL) assembly of polyelectrolyte films formed by alternate dipping of a charged surface into dilute solutions of a polycation and a polyanion.[3,4] This bottom-up strategy for the fabrication of soft nanostructured materials is poised to find practical applications in many areas.[5] It has also been the subject of theoretical investigations, and several models have been proposed to account for the properties of the multilayers formed by LbL deposition.[6−8] Abundant experimental evidence stresses the paramount importance of the chemical structure of the polyelectrolytes in controlling the properties of the multilayered films as well as the mechanism of their construction.[9−12] Early experiments focused on ubiquitous polyelectrolytes, such as poly(styrenesulfonate) and poly(allylamine hydrochloride).[4,13,14] More recently, the scope of the technique has been extended to such materials as polysaccharides, proteins, polynucleotides, enzymes, polypeptides, and

[†] Faculté de Pharmacie, Pavillon J. A. Bombardier.
[‡] Département de Chimie, Pavillon Roger-Gaudry.
[§] Center for Self-Assembled Chemical Structures.

(1) (a) Fleer, G. J.; Cohen Stuart, M. A.; Scheutjens, J. M. H. M.; Cosgrove, T.; Vincent, B. *Polymers at Interfaces*; Chapman & Hall: Cambridge, U.K., 1993. (b) Patra, C. N.; Chang, R.; Yethiraj, A. *J. Phys. Chem. B* **2004**, *108*, 9126−9132.
(2) Hara, M., Ed. *Polyelectrolytes: Science and Technology*; Dekker: New York, 1993.
(3) (a) Hammond, P. T. *Curr. Opin. Colloid Interfce Sci.* **2000**, *4*, 430−442. (b) Schonhoff, M. *Curr. Opin. Colloid Interface Sci.* **2003**, *8*, 86−95.
(4) Decher, G. *Science* **1996**, *277*, 1232−1237.
(5) (a) Decher, G., Schlenoff, J. B., Eds. *Multilayer Thin Films*; Wiley-VCH Verlag: Weinheim, Germany, 2002. (b) Hammond, P. T. *Adv. Mater.* **2004**, *16*, 1271−1293.
(6) (a) Schlenoff, J. B.; Dubas, S. T. *Macromolecules* **2001**, *34*, 592−598. (b) Castelnovo, M.; Joanny, J. F. *Langmuir* **2000**, *16*, 7524−7232.
(7) Messina, R. *Macromolecules* **2004**, *37*, 621−629.
(8) Lavalle, P.; Picart, C.; Mutterer, J.; Gergely, C.; Reiss, H.; Voegel, J.-C.; Senger, B.; Schaaf P. *J. Phys. Chem. B* **2004**, *108*, 635−648.
(9) (a) Arys, X.; Fischer, P.; Jonas, A. M.; Koetse, M. M.; Laschewsky, A.; Legras, R.; Wischerhoff, E. *J. Am. Chem. Soc.* **2003**, *125*, 1859−1865. (b) Schoeler, B.; Kumaraswamy, G.; Caruso, F. *Macromolecules* **2002**, *35*, 889−897. (c) Dubas, S. T.; Schlenoff, J. B. *Macromolecules* **1999**, *32*, 2, 8153−8160.
(10) Picart, C.; Mutterer, J.; Richert, L.; Luo, Y.; Prestwich, G. D.; Schaaf, P.; Vogel, J.-C.; Lavalle, P. *Proc. Natl. Acad. Sci. U.S.A.* **2002**, *99*, 12531−12535.
(11) Lavalle, P.; Gergely, C.; Cuisinier, F. J. G.; Decher, G.; Schaaf, P.; Voegel, J.-C.; Picart, C. *Macromolecules* **2002**, *35*, 4458−4465.
(12) Schoeler, B.; Poptoshev, E.; Caruso, F. *Macromolecules* **2003**, *36*, 5258−5264.

 10.1021/ja044385n CCC: $30.25

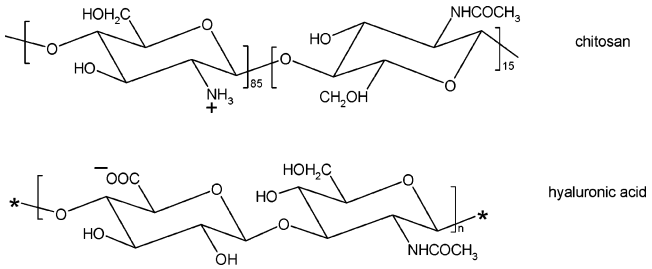

Figure 1. Structure of the polysaccharides used in this study.

various other biopolymers with the aim of creating functional biocompatible surfaces.[10,11,15−20] Recently, Thierry et al.[18] reported the assembly of polyelectrolyte multilayers onto arteries, as a means not only to protect an artery damaged during a revascularization procedure against blood coagulation but also to control the healing process by incorporating releasable bioactive molecules within the multilayer. This approach provides a powerful alternative to current minimum-invasive cardiovascular interventions.[21]

The polyelectrolytes selected for this study, hyaluronan and chitosan, are both polysaccharides. Hyaluronan (HA), a naturally occurring polyanion (solution $pK_a \approx 3.0$ [22]), is a linear polymer consisting of alternating *N*-acetyl-β-D-glucosamine and β-D-glucuronic acid residues linked (1→3) and (1→4), respectively (Figure 1). HA plays an important structural and mechanical role in various tissues, participates in the control of tissue hydration and water transport, and affects numerous biological processes, such as inflammation and tumor metastasis and development. Hyaluronan interacts with cells via specific receptor proteins, the hyaladherins, and it has been shown that several extracellular matrix HA-binding receptors are overexpressed in tumor cells or during the inflammation process, resulting in abnormally high levels of HA near tumor or inflammation sites.[23] Hyaluronan has found applications in drug delivery systems, medical imaging, cosmetic or nutritional formulations, and as a component in tissue engineering.[22]

Chitosan (CH), a random copolymer of *N*-acetyl-β-D-glucosamine and β-D-glucosamine linked (1→4), is obtained after partial *N*-deacetylation of chitin, a natural constituent of shell fish (Figure 1). Typically, in the case of commercial chitosans, only ∼15% of the sugar units are acetylated; the other sugar units bear free amine groups that are quaternized in acidic solution ($pK_a \approx 6.0$ [24]). CH is used in drug formulations, tissue engineering, and antibacterial treatments.[25]

The construction of polyelectrolyte multilayers is mainly driven by electrostatic interactions. Deposition of each polyelectrolyte leads to a net surface charge that attracts oppositely charged polyelectrolyte whose adsorption then leads to a surface charge reversal, hence allowing for further buildup. Taking a simplistic view, one expects that the mass or thickness of the multilayer increases linearly as a function of the number of polyelectrolyte bilayers. Linear growth has been confirmed experimentally in a number of cases, involving mostly strong polyelectrolyte pairs.[11,14,17] Weak polyelectrolytes, however, do not always follow this pattern. It can happen that the amount of polyelectrolyte deposited in each step is not constant throughout the multilayer buildup, but increases with the film thickness. This growth regime, termed "exponential growth", is commonly observed for polyelectrolyte pairs consisting of at least one polypeptide or polysaccharide; poly(L-lysine) (PLL)/alginate[19] and PLL/HA[8,10,16] pairs were the first reported examples. Other polyanion/polycation systems known to follow an exponential growth mechanism include poly(L-glutamic acid)/PLL,[8,11,26] poly(L-glutamic acid)/poly(allylamine),[27] poly(diallyldimethylammonium chloride)/poly(styrene sulfonate),[28] poly(acrylic acid)/poly(acrylamide-*co*-[3-(2-methyl-propionamido)-propyl]trimethylammonium chloride),[12] and HA/CH,[20] the system under investigation here. The driving force for exponential growth in poly(L-glutamic acid)/PLL,[8,11,26] PLL/HA,[8,10,16] and HA/CH[20] is the *diffusion* through the multilayer of at least one of the two polyelectrolytes, that together with their counterions, travel in and out of the multilayer without forming an electrostatic complex with the oppositely charged polyelectrolyte chains.[10,20,26] Theoretical modeling predicts that diffusion of the polyelectrolyte in and out of the film is (1) strongly related to the concentration of "fixed" charges (i.e. uncompensated polycation/polyanion pair charges) within the multilayer and (2) controlled by the difference between its chemical potential within the multilayer and in the aqueous phase.[8] Consequently, the amount of diffusing polyelectrolyte added during a deposition step exceeds the minimum amount needed to neutralize the surface charges of the multilayer it is brought in contact with and to create sufficient new charges (i.e. net surface charge) for further buildup. A nonlinear growth ensues as the amount of free, diffusing polyelectrolyte chains available for complexation in a given deposition step is proportional to the multilayer film thickness prior to the deposition.

(13) (a) Schmitt, J.; Grunewald, T.; Decher, G.; Pershan, P. S.; Kjaer, K.; Losche, M. *Langmuir* **1993**, *9*, 7058−7063. (b) Kaschak, D. M.; Lean, J. T.; Waraksa, C. C.; Saupe, G. B.; Usami, H.; Mallouk, T. E. *J. Am. Chem. Soc.* **1999**, *121*, 3435−3445.
(14) Caruso, F.; Niikura, K.; Furlong, D. N.; Okahata, Y. *Langmuir* **1997**, *13*, 3422−3426.
(15) (a) Chluba, J.; Voegel, J.-C.; Decher, G.; Erbacher, P.; Schaaf, P.; Ogier, J. *Biomacromolecules* **2001**, *2*, 800−805. (b) Serizawa, T.; Yamaguchi, M.; Akashi, M. *Biomacromolecules* **2002**, *3*, 724−731. (c) Caruso, F.; Mohwald, H. *J. Am. Chem. Soc.* **1999**, *121*, 6039−6046. (d) Burke, S. E.; Barrett, C. J. *Biomacromolecules* **2003**, *4*, 1773−1783. (e) Thierry, B.; Winnik, F. M.; Merhi, Y.; Silver, J.; Tabrizian, M. *Biomacromolecules* **2003**, *4*, 1564−1571. (f) Michel, M.; Vautier, D.; Voegel, J.-C.; Schaaf, P.; Ball, V. *Langmuir* **2004**, *20*, 4835−4839. (g) Rmaile, H. H.; Schlenoff, J. B. *J. Am. Chem. Soc.* **2003**, *125*, 6602−6603. (h) Constantine, C. A.; Mello, S. V.; Dupont, A.; Cao, X.; Santos, D., Jr.; Oliveira, O. N., Jr.; Strixino, F. T.; Pereira, E. C.; Cheng, T.-C.; Defrank, J. J.; Leblanc, R. M. *J. Am. Chem. Soc.* **2003**, *125*, 1805−1809. (i) Wood, K. C.; Boedicker, J. Q.; Lynn, D. M.; Hammond, P. T. *Langmuir* **2005**, *21*, 1603−1609. (j) Thierry, B.; Kujawa, P.; Tkaczyk, C.; Winnik, F. M.; Bilodeau, L.; Tabrizian, M. *J. Am. Chem. Soc.* **2005**, *127*, 1626−1627.
(16) Picart, C.; Lavalle, P.; Hubert, P.; Cuisinier, F. J. G.; Decher, G.; Schaaf, P.; Voegel, J.-C. *Langmuir* **2001**, *17*, 7414−7424.
(17) (a) Pei, R.; Cui, X.; Yang, X.; Wang, E. *Biomacromolecules* **2001**, *2*, 463−468. (b) Caruso, F.; Niikura, K.; Furlong, D. N.; Okahata, Y. *Langmuir* **1997**, *13*, 3427−3433.
(18) Thierry, B.; Winnik, F. M.; Merhi, Y.; Tabrizian, M. *J. Am. Chem. Soc.* **2003**, *125*, 7494−7495.
(19) Elbert, D. L.; Herbert, C. B.; Hubbell, J. A. *Langmuir* **1999**, *15*, 5355−5362.
(20) Richert, L.; Lavalle, P.; Payan, E.; Shu, X. Z.; Prestwich, G. D.; Stoltz, J.-F.; Schaaf, P.; Voegel, J.-C.; Picart, C. *Langmuir* **2004**, *20*, 448−458.
(21) Groth, T.; Lendlein, A. *Angew. Chem.* **2004**, *43*, 926−928.
(22) Lapcík, L., Jr.; Lapcík, L.; De Smedt, S.; Demeester, J.; Chabrecek, P. *Chem. Rev.* **1998**, *98*, 2663−2684.
(23) (a) Arrufo, A.; Stamenkovic, I.; Melnick, M.; Underhill, C.; Seed, B. *Cell* **1990**, *61*, 1303−1304. (b) Agre, U.; Tölg, C.; Paiwand, F.; Turley, S. A.; Harrison, R.; Turley, E. A. In *Redefining Hyaluronan*; Abatangelo, G., Weigel, P. H., Eds.; Elsevier: Amsterdam, 2000; pp 63−76, and references therein.
(24) Rinaudo, M.; Pavlov, G.; Desbrieres, J. *Polymer* **1999**, *40*, 7029−7032.
(25) Janes, K. A.; Calvo, P.; Alonso, M. J. *Adv. Drug Delivery Rev.* **2001**, *47*, 83−97.
(26) Lavalle, P.; Vivet, V.; Jessel, N.; Decher, G.; Voegel, J.-C.; Mesini, P. J.; Schaaf, P. *Macromolecules* **2004**, *37*, 1159−1162.
(27) Boulmedais, F.; Ball, V.; Schwinte, P.; Frisch, B.; Schaaf, P.; Voegel, J.-C. *Langmuir* **2003**, *19*, 440−445.
(28) McAloney, R. A.; Sinyor, M.; Dudnik, V.; Goh, M. C. *Langmuir* **2003**, *17*, 6655−6663.

On the basis of a confocal laser scanning microscopy investigation of HA/CH multilayers constructed with fluorescently labeled polysaccharides, Richert et al. attributed the exponential growth of HA/CH to the diffusion through the multilayer of CH, but not of HA.[20] An in-situ atomic force microscopy (AFM) investigation of the layer-by-layer morphology of HA/CH[20] revealed that the film buildup proceeds in two stages. The surface is initially covered with isolated islets, whose formation has also been predicted by computer simulations.[7] These islets grow in size and coalesce as new polyelectrolyte is adsorbed onto and between them. In the second stage, the islands interconnect, leading to a vermiculate morphology, and eventually, to an almost uniform film as more polyelectrolyte layers are deposited. Measurements of the contact angles of the surface islands suggest that although these are more or less compositionally homogeneous at each stage of the buildup, there is a continuous evolution of the polyelectrolyte composition of the islands and, hence, a restructuring of the material at the surface.[16,20] Richert et al. also used in-situ quartz crystal microbalance (QCM) measurements to evaluate the effect of the size of chitosan on the growth kinetics using HA/CH pairs formed by a HA sample of molecular weight (MW) 400 000 and three CH samples ranging in MW from 110 000 to 460 000.[20] In a QCM experiment, changes in the crystal resonance frequency are observed as a function of polyelectrolyte adsorption on the crystal surface. On the basis of QCM frequency shifts, it appears that thicker films form for the HA/CH pair with the CH of lowest MW (110 000).[20] However, the viscoelasticity of the HA/CH multilayer, which also contributes to the measured frequency change, will also depend on the molar mass of CH, a situation that complicates the interpretation of the QCM data. Despite recent advances in QCM instrumentation, it remains difficult to separate these two effects, so that larger frequency changes are not necessarily indicative of thicker films (or of a greater mass of adsorbed polymer).[29] More careful measurements are therefore required, especially since there have been only a few investigations of the effect of MW on the assembly of polyelectrolyte multilayers.[30]

In the present work, we use surface plasmon resonance spectroscopy (SPR), together with AFM, to investigate the LbL buildup of HA/CH multilayers. Like QCM, SPR spectroscopy is a noninvasive evanescent wave technique which is capable of measuring film thicknesses with a resolution on the angstrom to nanometer scale.[31] Early work by Knoll et al. demonstrated that SPR can be a powerful tool for in-situ real-time monitoring of the adsorption behavior of charged macromolecules during LbL buildup and for the quantitative determination of the thickness of each deposited layer.[32] We exploit SPR and AFM to assess the effect of the MW of *both* the diffusing and nondiffusing polyelectrolyte on the exponential growth of the multilayers using samples differing by *1 order of magnitude* in terms of intrinsic MW (Table 1). The study was prompted in part by the fact that, in vivo, the biological activity of HA depends strikingly on its size.[33] For example, high MW HA inhibits angiogenesis, whereas oligomers of HA induce angiogenesis.[34] Thus, our findings may lead to the design of HA/CH nanocoatings endowed with specific biological activity depending on the size of the HA employed during the multilayer construction.

Table 1. Characteristics of the Polysaccharides Employed in This Study

polysaccharide	M_n[a,b]	M_w[a,b]	M_w/M_n[a]	R_g[b] (nm)	degree of deacetylation (%)[c]
HA-360K	360 000	680 000	1.9	66[a]	
HA-31K	31 000	47 000	1.5	19[a]	
CH-160K	160 000	260 000	1.6	77[d]	85
CH-30K	30 000	84 000	2.8	27[d]	81

[a] From GPC measurements (see Experimental Section for details). [b] M_n = number-average molecular weight; M_w = weight-average molecular weight; R_g = radius of gyration. [c] Degree of deacetylation measured by ^{1}H NMR and UV−visible spectroscopy.[45] [d] From light scattering experiments (see Experimental Section for details).

Results and Discussion

(A) Methodology: Polyelectrolytes and Surfaces. Fully ionized HA and CH (Figure 1) behave in solution as stiff chains with a persistence length of the order of 6−12 nm for CH and ∼6 nm for HA.[20] Note that HA bears one carboxylate ion or negative charge per *di*saccharide unit, whereas chitosan, with a deacetylation degree of 85%, has one ammonium group or positive charge per ∼1.2 saccharide units. Thus, equimolar quantities of CH and HA, expressed in terms of saccharide units, are not matched in terms of ionic charge, a situation that affects the morphology of the multilayer and the molecular weight dependence of the multilayer thickness, as shown previously in a study of partially ionized poly(acrylic acid)/poly(allylamine hydrochloride).[35]

Our two samples of HA differ by a factor of ∼10 in number average MW, whereas the samples of chitosan differ by a factor of ∼5 in M_n (Table 1). Polysaccharides more closely matched in molecular weight, i.e., HA-360K/CH-160K and HA-31K/CH-30K, were assembled, as well as polymers mismatched in size, i.e. HA-31K/CH-160K and HA-360K/CH-30K. As depicted in Figure 2, HA/CH multilayers were built on positively charged surfaces generated by the adsorption of a polyethyleneimine (PEI) layer on gold-coated LaSFN9 glass slides modified with a negatively charged self-assembled monolayer of a carboxylic acid-terminated alkylthiol, 11-mercaptoundenanoic acid (MUA).

(B) AFM Imaging of HA/CH Multilayering. The evolution of the film morphology and thickness during the assembly of up to 12 bilayers of the high-MW and low-MW pairs, HA-360K/CH-160K and HA-31K/CH-30K, were followed in situ by AFM. Key images depicting different stages in the alternate adsorption of HA and CH layers are presented in Figure 3. For both HA/CH pairs, we observe a progression from smaller isolated islets to larger islands and vermiculate patterns with increasing number of deposited bilayers, consistent with previous reports.[16,20] For the case of the high-MW polysaccharides, our results are qualitatively similar to those obtained by Richert et

(29) Vogt, B. D.; Lin, E. K.; Wu, W.; White, C. C. *J. Phys. Chem. B* **2004**, *108*, 12685−12690.
(30) (a) Sui, Z.; Salloum, D.; Schlenoff, J. B. *Langmuir* **2003**, *19*, 2491−2495. (b) Dubas, S. T.; Schlenoff, J. B. *Macromolecules* **2001**, *34*, 3736−3740. (c) Schwarz, S.; Nagel, J.; Jaeger, W. *Macromol. Symp.* **2004**, *211*, 201−216.
(31) For reviews of SPR theory and experimental considerations, see: (a) Davies, J.; Faulkner, I. In *Surface Analytical Techniques for Probing Biomaterial Processes*; Davies, J., Ed.; CRC Press: Boca Raton, FL, 1996; pp 67−87. (b) Knoll W. *Annu. Rev. Phys. Chem.* **1998**, *49*, 569−638.
(32) Advincula, R.; Aust, E.; Meyer, W.; Knoll, W. *Langmuir* **1996**, *12*, 3536−3540.
(33) Toole, B. P. *Nature Rev. Cancer* **2004**, *4*, 528−539.
(34) Rooney, P.; Kumar, S.; Ponting, J.; Wang, M. *Int. J. Cancer* **1995**, *60*, 632−636.
(35) Shiratori, S. S.; Rubner, M. F. *Macromolecules* **2000**, *33*, 4213−4219.

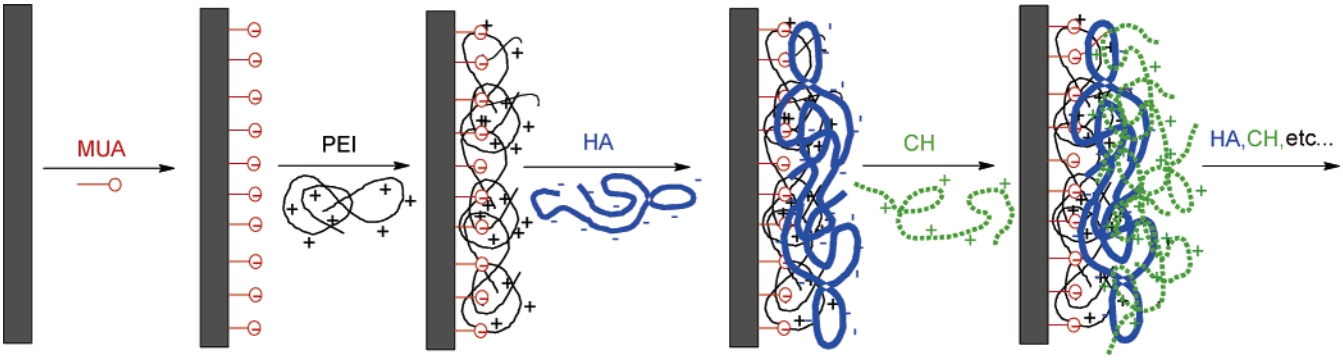

Figure 2. Schematic representation of the multilayer film formation.

al. for HA and CH of comparable MWs (400 000 and 110 000, respectively) and degree of CH deacetylation.[20] We also observe significant differences in the evolution and dimensions of the surface structures as a function of the MWs of the HA and CH. We focus herein on these novel findings.

Following the adsorption of HA and then CH (Figure 3A,B, $n = 1$) onto the PEI-coated MUA−Au substrate (root-mean-square (RMS) roughness of ∼1.4 nm), the surface is covered with isolated globular clusters ∼20−40 nm in height and ∼100−180 nm in width, although the measured width is overestimated due to AFM tip convolution effects[36] (typical radius of curvature of 20 nm). These globules are likely coils of single CH molecules that are electrostatically complexed to the underlying layer of HA, given that their size is comparable to the radius of gyration of the chitosans used for the layer-by-layer buildup (Table 1) and that no distinct HA structures[37] were detected after deposition of the first HA-360K or HA-31K layer (Figure S1, Supporting Information). CH may also be adsorbed (in loop, train, and tail configurations) to the underlying HA layer in the regions between the clusters. Deposition of the second layers of HA and CH already results in the surface being densely covered with larger spheres, ∼230−285 nm in width, for the high-MW pair (Figure 3A, $n = 2$). By contrast, the surface is only partly covered with larger spherical islets, ∼160−230 nm in width, after deposition of the second layers of HA-31K and CH-30K (Figure 3B, $n = 2$). For both the high- and low-MW polysaccharides, the polyelectrolyte islands grow in size and lose their spherical shape as the multilayer buildup is continued to five bilayers (Figure 3A,B, $n = 5$). At this stage, the island widths are comparable (∼335−570 nm for HA-360K/CH-160K vs ∼380−605 nm for HA-31K/CH-30K). The average height of the islands is larger in the case of the HA-31K/CH-30K pair (186 ± 39 nm vs 121 ± 24 nm) so that PEI−$(HA/CH)_5$ films formed from the low-MW HA and CH are rougher (RMS roughness ≈ 61 nm) than those assembled from the high-MW polysaccharides (RMS roughness ≈ 30 nm). The islands interconnect to form larger vermiculate structures as the buildup proceeds. The transition to a vermiculate morphology occurs between the deposition of the 5th and 8th bilayers for HA-360K/CH-160K and between the 8th and 10th bilayers for HA-31K/CH-30K (Figure 3A,B). The wormlike domains are of the order of 1 μm across (narrowest part) and 389 ± 26 nm in height for PEI−$(HA\text{-}31K/CH\text{-}30K)_{10}$ (Figure 3B), making these considerably larger than those of the high-MW PEI−$(HA/CH)_{10}$ (∼0.5−1 μm across and 184 ± 62 nm in height, Figure 3A). Furthermore, the surface of the wormlike domains is smoother in the case of the low-MW polyelectrolyte multilayer as compared to the high-MW one (Figure 3A,B, $n = 8$ and $n = 10$). In fact, for the PEI−$(HA\text{-}360K/CH\text{-}160K)_8$ film, distinct globular features 250−600 nm in width and 20−50 nm in height can be seen in the high-magnification image (Figure 3A, inset $n = 8$). The small globular structures are either aggregates of CH (multilayer terminating in CH), as suggested above for PEI−$(HA/CH)_1$, or clusters of HA/CH complexes.[12,16,38]

HA complexes with both surface-complexed CH and with CH that diffuses out of the film upon exposure of a CH-terminated multilayer to HA solution. The surface morphologies of HA- and CH-terminated films may therefore show some fine structural differences. Since this issue has not been specifically addressed in other AFM studies,[14,16,20,28,39,40] we imaged high- and low-MW films between the depositions of the 8th and 10th /11th HA and CH layers (Figure S2, Supporting Information). The surface morphologies of the HA- and CH-terminated multilayers were very similar. Finally, we note that the deposition of additional polyelectrolyte layers leads to even larger structures for the HA-31K/CH-30K polyelectrolyte pair (Figure 3B, $n = 12$).[41] The RMS roughnesses of the high- and low-MW PEI−$(HA/CH)_{12}$ films are ∼110 nm and ∼131 nm, respectively.

Holes could be effectively created in multilayer films of the low- and high-MW polysaccharides by repeatedly scanning a small area under "hard" tapping conditions (Figure S3, Supporting Information). While the removal of organic material by scanning an AFM tip with a high applied force is a common practice for film thickness determinations, this is usually accomplished in contact mode and not with the less intrusive tapping mode used for imaging in this work. In their AFM investigation of the polyelectrolyte multilayer film morphology, McAloney et al. point out that the ability to scrape off polymer from the surface in tapping mode suggests a loose association of the polyelectrolyte layers.[40] Such a loose film structure for

(36) Markiewicz, P.; Goh, M. C. *Langmuir* **1994**, *12*, 5−7.
(37) (a) Cowman, M. K.; Li, M.; Dyal, A.; Balazs, E. A. *Carbohydr. Polym.* **2000**, *41*, 229−235. (b) Cowman, M. K.; Li, M.; Balazs, E. A. *Biophys. J.* **1998**, *75*, 2030−2037.
(38) Menchaca, J.-L.; Jachimska, B.; Cuisinier, F.; Perez, E. *Colloids Surf., A* **2003**, *222*, 185−194.
(39) (a) Voigt, U.; Jaeger, W.; Findenegg, G. H.; von Klitzing, R. *J. Phys. Chem. B* **2003**, *107*, 5273−5280. (b) Mermut, O.; Lefebvre, J.; Gray, D. G.; Barrett, C. J. *Macromolecules* **2003**, *36*, 8819−8824.
(40) McAloney, R. A.; Dudnik, V.; Goh, M. C. *Langmuir* **2003**, *19*, 3947−3952.
(41) AFM imaging is more difficult at this stage (for both HA-360K/CH-160K and HA-31K/CH-30K). Picart et al. attribute this difficulty to larger fluctuations in the local charge density in the thicker films than in the initial layers; see ref 16.

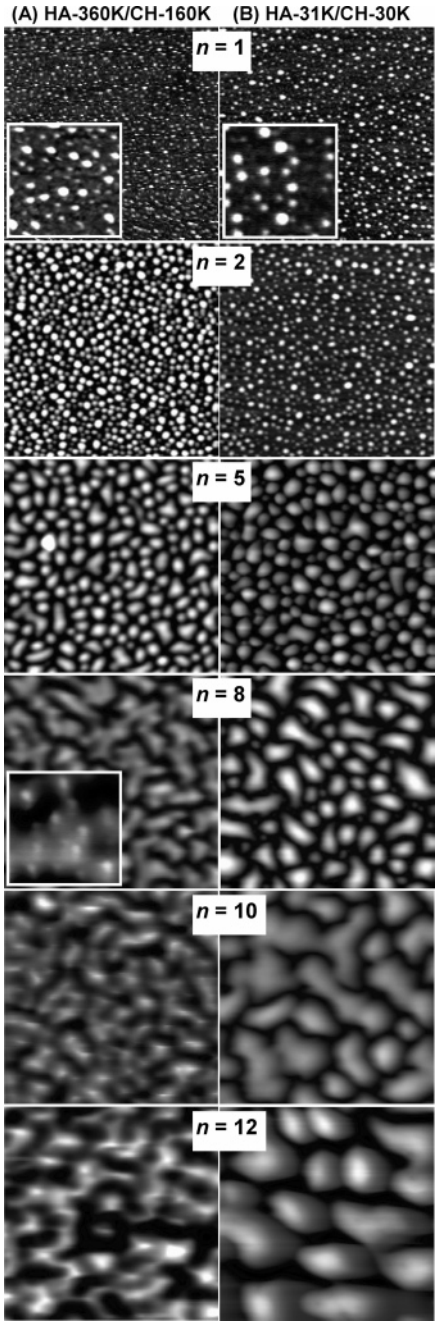

Figure 3. AFM topography images (7.5 μm × 7.5 μm) acquired in 0.15 M NaCl solution (pH 4.5) for different steps of the alternate deposition of high-MW (panel A) and low-MW polysaccharides (panel B) onto a PEI-coated MUA−Au substrate. *n* indicates the number of HA/CH bilayers deposited. The insets shown in panels A and B for $n = 1$ are 1.5 μm × 1.5 μm magnifications, while the inset in panel A for $n = 8$ is a 2.5 μm × 2.5 μm magnification. Maximum height or *z*-ranges in panel A are 35 ($n = 1$), 90 ($n = 2$), 225 ($n = 5$), 500 ($n = 8$), 500 ($n = 10$), and 600 nm ($n = 12$). Maximum *z*-ranges in panel B are 35 ($n = 1$), 150 ($n = 2$), 400 ($n = 5$), 400 ($n = 8$), 700 ($n = 10$), and 850 nm ($n = 12$).

HA/CH would be consistent with the postulated presence of free mobile CH chains and salt ions inside the film and the partial exchange of free CH with HA-complexed CH.[20] Scratching the PEI−(HA-360K/CH-160K)$_5$ film (Figure 3A, $n = 5$) yields an average thickness of 120 ± 43 nm (Table 2), the magnitude of the standard deviation reflecting the substantial height amplitude of the film profile. The PEI−(HA-360K/CH-160K)$_5$ film is therefore continuous but quite rough. In fact, due to the peaks (and later ridges) and valleys formed by the interfacial island structures, the multilayer films continue to exhibit significant thickness modulations and surface roughnesses as more bilayers are deposited. For instance, the PEI−(HA-360K/CH-160K)$_8$ film is 284 ± 99 nm thick and its RMS roughness is ~60 nm. The islands and vermiculate structures (that appear later on in the multilayer buildup) provide an increased surface area that may facilitate CH diffusion into the HA/CH films. Scratching the 12 bilayer films yields an average thickness of 869 ± 202 nm for HA-360K/CH-160K and 448 ± 202 nm for HA-31K/CH-30K (Table 2).

Table 2. HA/CH Multilayer Thicknesses Measured by AFM

HA/CH pair	bilayer no.	d_{film} [a] (nm)
HA-360K/CH-160K	5	115 ± 45 ($n = 301$)
		125 ± 40 ($n = 267$)
HA-360K/CH-160K	8	279 ± 98 ($n = 240$)
		294 ± 100 ($n = 127$)
HA-360K/CH-160K	12	824 ± 151 ($n = 113$)
		926 ± 241 ($n = 87$)
HA-31K/CH-30K	12	448 ± 202 ($n = 133$)

[a] The film thickness (d_{film}) was determined from step heights measured between the bottom of the indentation created with the AFM tip to the upper surface of the film. Step heights are the average values of many measurements at different points (number indicated in parentheses) along 8−12 different linear cross-sections. AFM images used for step height measurements were fitted with a third-order plane calculated for the entire image area.

In summary, AFM imaging of HA/CH multilayers at various stages of the buildup indicates that (1) a PEI−(HA-360K/CH-160K)$_{12}$ film is twice as thick as a PEI−(HA-31K/CH-30K)$_{12}$ film, (2) full coverage of the surface with spherical polyelectrolyte islets as well as the progression from a morphology consisting of isolated islands to interconnected or vermiculate domains occurs after the deposition of fewer layers in the case of the high- vs low-MW pair, and (3) much larger structures are present in the low-MW PEI−(HA-31K/CH-30K) after the transition from individual islands to interconnected domains compared with the high-MW polyelectrolyte multilayer. These differences in surface morphology may be an indication of differences in the bulk composition of the multilayer, particularly the degree of hydration of the polymer chains. The SPR study described next confirms this hypothesis, as do assessments of the QCM dissipation factors conducted in our laboratory, which indicate that the low-MW constructs are more gel-like than their high-MW counterparts. The different surface morphologies and degree of hydration/swelling of multilayers constructed from high- and low-MW HA and CH should allow one to tailor the bioadhesive properties of films through the choice of polysaccharide MW.[19,20]

(C) SPR Characterization of Multilayer Buildup. Two approaches were taken to monitor the film construction via SPR. First, the polyelectrolyte adsorption kinetics were followed by tracking the change in the resonance angle with time ($\Theta_m - t$ curves), polyelectrolyte adsorption and film growth giving rise to positive shifts in Θ_m. In this mode, one can assess the following: (1) the time required to reach saturation coverage upon injection of a polyelectrolyte solution and (2) the changes in the adsorbed film thickness upon rinsing a newly deposited polyelectrolyte layer with aqueous NaCl solution. Second, after each polyelectrolyte deposition/NaCl rinse step, angular reflectivity curves ($R - \Theta$) were recorded and fit to a multilayer Fresnel

model to obtain the optical film thickness with increasing bilayer number.

(1) Kinetics of Multilayer Formation. The change in the angle of minimum reflectivity Θ_m was monitored during the alternate adsorption of 12 layers of HA and CH. The same sequence of depositions was carried out with all four HA/CH pairs of different MWs. Kinetic curves recorded for the four pairs (Figure 4) followed the same general trend: an initial stepwise increase in Θ_m with each successive deposition of HA and CH followed by a leveling off of Θ_m after 8−10 bilayers. However, a detailed analysis of the individual kinetic curves unveiled a number of important differences, as discussed in the following sections.

For the buildup of bilayers 1−4, a rapid increase in Θ_m, which reached a constant value after 5 min, was observed upon injection of HA (Figure 4A, HA1−HA4) or CH (Figure 4A, CH1−CH4) solution. Flushing the SPR cell with NaCl solution resulted in a small decrease in Θ_m, attributable to desorption of some polyelectrolyte from the surface. A new pattern emerged during construction of the 5th and 6th bilayers (Figure 4B); while the injection of HA still triggered a shift in Θ_m ($\Delta\Theta_{HA}$) of similar magnitude to that observed during buildup of the initial bilayers, injection of CH induced a significantly smaller increase of Θ_m ($\Delta\Theta_{CH}$), compared to the $\Delta\Theta_m$ triggered by the injection of HA. This difference between $\Delta\Theta_{HA}$ and $\Delta\Theta_{CH}$ appears during the formation of the 5th bilayer in the case of polyelectrolyte pairs consisting of the low-MW HA sample (HA-31K/CH-30K and HA-31K/CH-160K), but only during buildup of the 6th bilayer in the case of pairs consisting of high-MW HA (HA-360K/CH-160K and HA-360K/CH-30K). The subsequent addition of HA (Figure 4B, HA6 or HA7, respectively) resulted in a further increase of Θ_m. This means that despite the smaller increase in resonance angle measured for deposition of the preceding CH layer (CH5 or CH6), a reversal of the net surface charge occurred, permitting further buildup of the 6th or 7th bilayer. The smaller magnitude of $\Delta\Theta_{CH}$ can result from one or more of the following effects, addressed in the paragraphs below: (1) deposition of a thinner layer of CH or loss of adsorbed material, (2) change in the film optical properties due to swelling/hydration, or (3) restructuring of the multilayer.

During the formation of the 8th bilayer (Figure 4B), injection of HA still triggered a positive $\Delta\Theta_m$ (e.g. 0.73° for HA-360K and 0.65° for HA-31K), but injection of CH now resulted in a negative $\Delta\Theta_m$ (e.g. −0.48° for CH-160K and −0.13° for CH-30K). Subsequent rinsing with aqueous NaCl caused a partial recovery of the resonance angle, but its value remained lower than that of the preceding HA deposition step. This pattern repeated itself upon further buildup (bilayers 9−12, Figure 4C); Θ_m increases after the addition of HA, then decreases upon the next addition of CH, and increases once again upon rinsing, but does not return to the value attained at the end of the previous HA deposition step. Moreover, beginning with the 9th bilayer for the high-MW pair (HA-360K/CH-160K), the 10th bilayer for the mismatched pairs (HA-31K/CH-160K and HA-360K/CH-30K), and the 11th bilayer for the low-MW pair (HA-31K/CH-30K), a cyclical evolution of the resonance angle emerges; Θ_m adopts similar values at the end of each HA addition/rinsing and CH addition/rinsing steps. We also observe an initial overshoot of Θ_m upon addition of HA, beginning with the deposition of the 9th and 11th/12th bilayer for the HA/CH pairs consisting of the high-MW HA and low-MW HA, respectively. This overshoot becomes more pronounced with each successive bilayer.

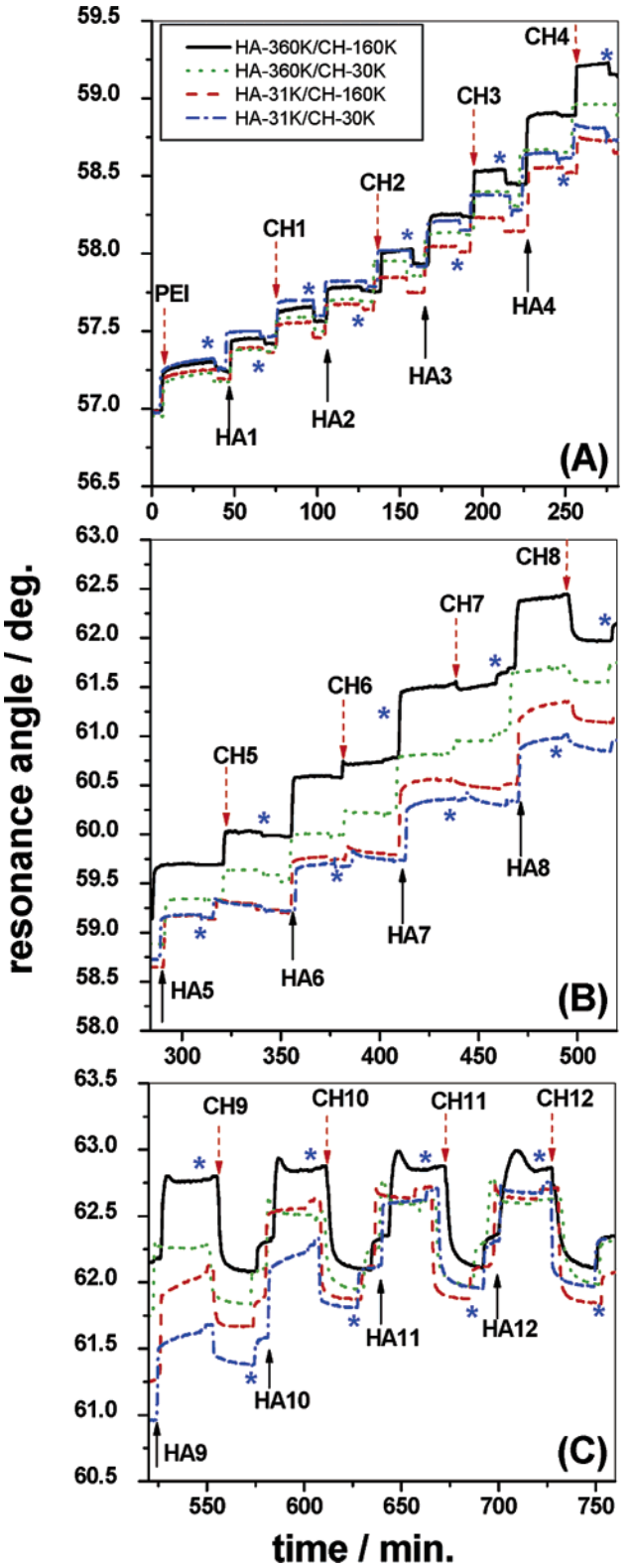

Figure 4. Changes of the SPR resonance angle (Θ_m) as a function of time during the buildup of HA/CH multilayers with polysaccharides of different molecular weights: construction of (A) first 4 bilayers, (B) 5−8 bilayers, and (C) 9−12 bilayers. Black arrows indicate the injection of HA. Red arrows indicate the injection of PEI or CH. The blue stars point to the injection of aqueous NaCl (0.15 M, pH 4.5).

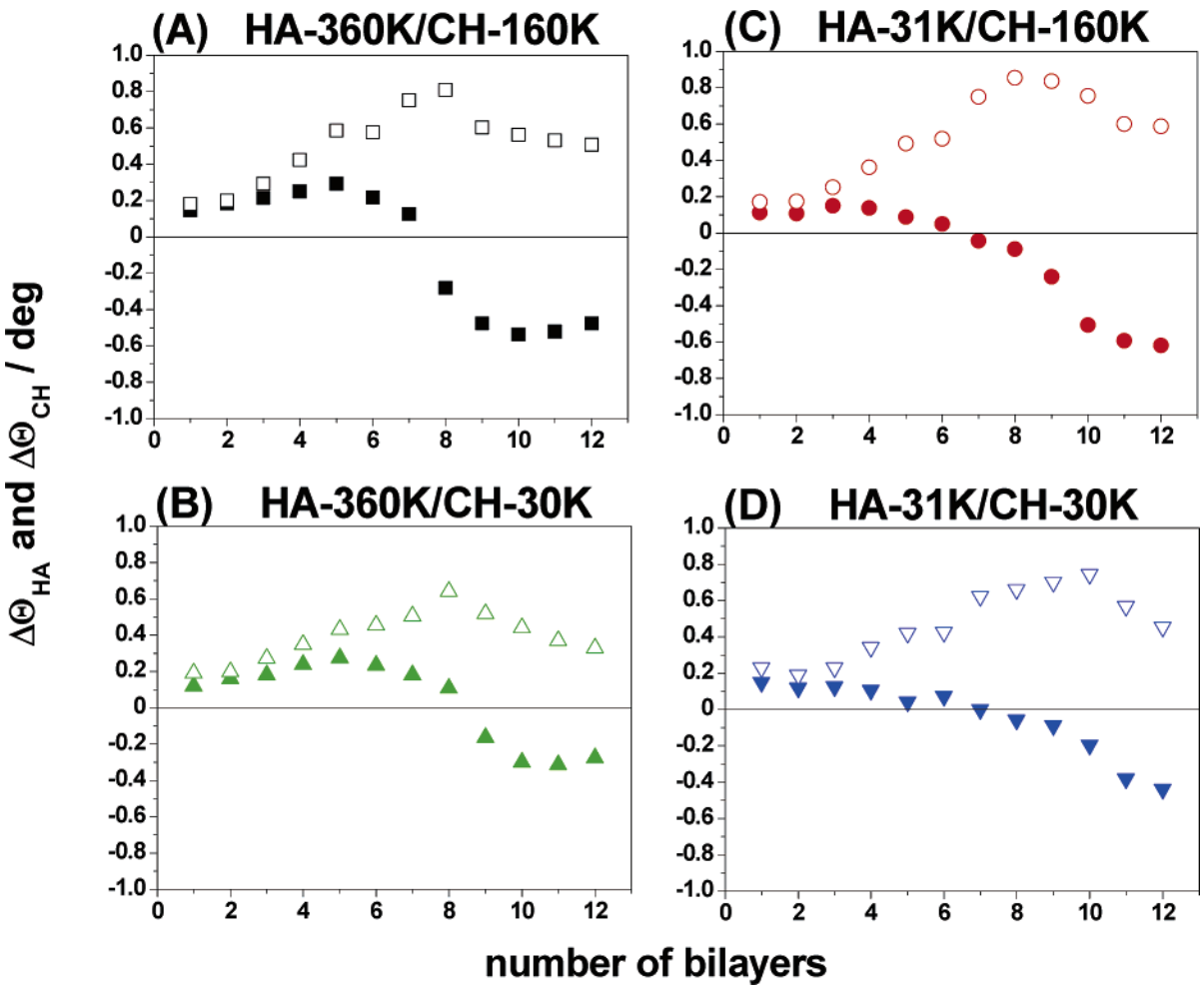

Figure 5. Shifts in the SPR resonance angle as a function of the number of bilayers after the deposition of HA ($\Delta\Theta_{HA}$, open symbols) and CH ($\Delta\Theta_{CH}$, filled symbols): (A) HA-360K/CH-160K; (B) HA-360K/CH-30K; (C) HA-31K/CH-160K; and (D) HA-31K/CH-30K.

The periodic variation of Θ_m and negative $\Delta\Theta_{CH}$ values recorded for the 8−12 bilayer region are not due to the dissolution/loss of adsorbed HA/CH complex and cessation of the film growth since the average film thickness measured by AFM for HA-360K/CH-160K increases from ∼280−290 nm for an 8 bilayer film to ∼800−900 nm for a 12 bilayer construct (Table 2). A cyclical evolution of the effective refractive index signal, such as the one reported above for the resonance angle, was also observed during the buildup of HA/PLL[16] and HA/CH[20] multilayers via optical waveguide light mode spectroscopy (OWLS), another evanescent wave technique sensitive to both the thickness and refractive index of an adsorbed layer. It is due to the fact that the growing film/water interface eventually moves beyond the distance of ∼200−300 nm typically probed by the evanescent wave in SPR and OWLS.[42] In the case of the HA/CH pairs investigated herein, the film thicknesses become greater than the probe depth of surface plasmons in the region encompassing the buildup of 8−12 bilayers. Any observed signal changes detected for deposition of HA and CH are therefore attributable to changes in the film refractive index (n_{film}) or dielectric constant ($\epsilon_{film} = (n_{film})^2$) resulting from the diffusion of CH in and out of the 200−300 nm region nearest to the gold surface and accompanying film swelling/deswelling.[10,16,20] A Fresnel analysis of the $R-\Theta$ scans indicates that ϵ_{film} oscillates between ∼1.900 and 1.910 for deposition of HA layers and between ∼1.885 and 1.900 for deposition of CH layers. The ϵ_{film} values are fairly independent of the polysaccharide MWs (Figure S4, Supporting Information) and closely match those reported by Richert et al.[20] in their study of HA/CH with MWs similar to those of the HA-360K and CH-160K samples.

To follow more accurately the effect of the polysaccharide MWs on the evolution of $\Delta\Theta_{HA}$ and $\Delta\Theta_{CH}$ with the number of deposited bilayers, the shifts in Θ_m after each HA and CH deposition/rinse step were determined from *full* angular reflectivity scans for all four HA/CH pairs. The $\Delta\Theta_{HA}$ values (always positive) follow the same trend for all four pairs and peak around 8−9 deposited bilayers (Figure 5). By contrast, the plots of $\Delta\Theta_{CH}$ vs the number of bilayers show clear differences in the evolution of $\Delta\Theta_{CH}$ that depend on the MW of HA, the nondiffusing species, and not on that of CH, the diffusing species. During construction of the four mutilayers, $\Delta\Theta_{CH}$ initially remains either constant (Figure 5C,D) or increases slightly (Figure 5A,B) with increasing bilayer number and then decreases before reaching a nearly constant negative value. The

(42) The characteristic decay length of the evanescent field in our SPR experiments is ∼234 nm for 633 nm light (∼37% of the light wavelength); see e.g.: Jung, L. S.; Campbell, C. T.; Chinowsky, T. M.; Mar, M. N.; Yee, S. S. *Langmuir* **1998**, *14*, 5636−5648. The resonance angle calculated using an average ϵ_{film} value of 1.899 for the polyelectrolyte multilayer and the five layer model described in the Experimental Section tends toward a limiting value for thicknesses ≥ 290 nm.

crossover from positive to negative $\Delta\Theta_{CH}$ values is related, in all cases, to the film thickness extending beyond the detection threshold of SPR and decrease in ϵ_{film} discussed above. This crossover takes place across the span of ca. two bilayers for the high-MW HA pairs (Figure 5A,B): from the 7/8th to 9/10th bilayer. We note, however, that the pairs consisting of the low-MW HA (Figure 5C,D) exhibit a more gradual transition from positive to negative values of $\Delta\Theta_{CH}$ (i.e. across the 6th−11th bilayers). The film dielectric constants corresponding to the addition of CH being similar for all four pairs, the more gradual nature of the positive-to-negative $\Delta\Theta_{CH}$ transition can be explained by the multilayer film thickness increasing less rapidly in the case of the low- vs the high-MW HA pairs. For example, the optical film thickness of HA-360K/CH-160K (Figure 5A) increases 3-fold, from 109 nm for 6 bilayers to 297 nm (SPR detection threshold) for 8 bilayers. By comparison, the HA-31K/CH-160K film thickness (Figure 5C) only doubles across the 6−8 bilayer span (from 72 to 158 nm). These results suggest a faster growth rate for multilayers formed from high-MW HA (which will be discussed in more detail in the next section). The abrupt vs gradual nature of the positive-to-negative $\Delta\Theta_{CH}$ crossover may also be caused by structural film rearrangements; AFM images of the high- and low-MW HA/CH pairs showing a shorter island growth and coalescence stage as well as an earlier transition from islands to a vermiculate morphology for the high-MW multilayer compared to the low-MW one (Figure 3).

(2) Multilayer Film Thicknesses. SPR scans collected for the growing multilayers were analyzed using the five-layer optical model described in the Experimental Section. Each HA/CH film was modeled as a single layer since HA/CH multilayers exhibit an intermeshed, rather than a layered structure, with continual restructuring as the film grows.[10,20,26] We used either an average film dielectric constant (value 1.899, open symbols, Figure 6) or separate values for HA- and CH-terminated layers (1.904 and 1.893, respectively, filled symbols, Figure 6) to obtain the total film thickness after the addition of each polyelectrolyte layer. Since the structures of the two polysaccharides are quite similar (Figure 1), the dielectric constants or refractive indices of HA and CH layers in water are expected to be very similar. The close agreement between the AFM and SPR film thicknesses for 5 and 8 bilayer films of HA-360K/CH-160K demonstrates that either choice of ϵ_{film} is quite reasonable. Optical thicknesses were determined only for films consisting of fewer than 10 HA/CH bilayers (d_{film} < 250 nm). As revealed by the AFM images, the HA/CH multilayers show strong thickness modulations; the apparent thickness determined by SPR is the average over the film profile.

Overall, and in agreement with observations based on QCM measurements,[20] plots of the optical film thickness vs the number of deposited bilayers exhibit an exponential growth behavior (Figure 6).[43] During the initial stage of multilayer construction, i.e., bilayers 1−3, the film thickness increment per deposition is small and of the same magnitude (~3 nm per layer), regardless of the MWs of the polyelectrolytes. This situation changes, however, as the buildup continues and a steep growth

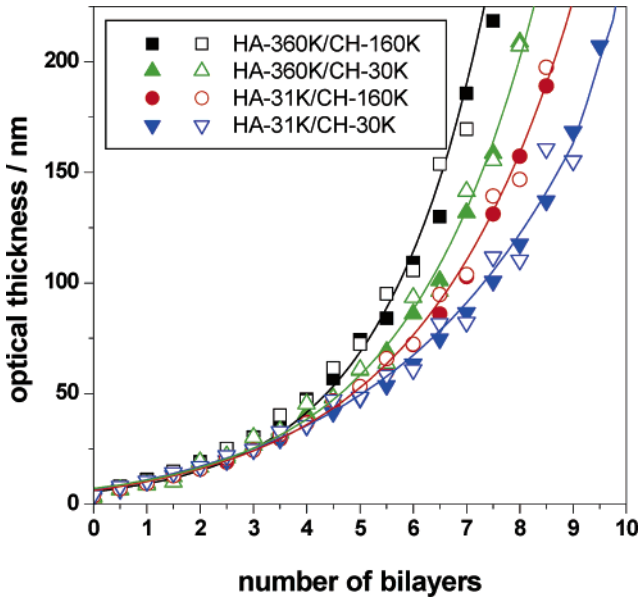

Figure 6. Optical thickness vs number of bilayers calculated using the Fresnel equations and film dielectric constants of 1.904 and 1.893 for HA- and CH-terminated layers, respectively (filled symbols) or an average value of 1.899 (open symbols). The lines represent exponential fits of the data points to the equation $y = a\exp(bx) + c$. The exponent b-parameter values obtained from the fits are as follows: HA-360K/CH-160K, 0.5090 ± 0.0584; HA-360K/CH-30K, 0.5110 ± 0.0464; HA-31K/CH-160K, 0.5074 ± 0.0326; and HA-31K/CH-30K, 0.4050 ± 0.1222. The a-parameter values obtained from the fits are as follows: HA-360K/CH-160K, 8.2; HA-360K/CH-30K, 5.8; HA-31K/CH-160K, 4.3; and HA-31K/CH-30K, 3.2.

regime (exponential) prevails.[44] The crossover between the two regimes depends on the MWs of *both* polyelectrolytes. It occurs after the deposition of ~2 bilayers, for HA-360K/CK-160K, but only after the deposition of ~3 bilayers, in the case of the HA-31K/CH-30K pair (i.e. bilayer numbers for which the plots of ln of the optical thickness vs number of bilayers become linear). The number of bilayers for which the crossover occurs for the high- (~2) and low- (~3) MW pairs coincides with the stage in the multilayer buildup at which the film surface is fully covered with polyelectrolyte complex (Figure 3), resulting in a more effective CH diffusion. Beyond this crossover region, the thickness increment per layer is large. The film thickness at a given number of deposition steps (i.e. bilayers 5−9) decreases in the following order: HA-360K/CH-160K > HA-360K/CH-30K > HA-31K/CH-160K > HA-31K/CH-30K. Fits of the data points to an exponential law of the type $y = a\exp(bx) + c$ (where y is the optical film thickness, x is the number of HA/CH bilayers, b reflects the rate of film growth, and a defines the point at which a steep growth is initiated)[10,20,26] yield similar values of the exponent b (average value of 0.48 ± 0.09) for the four MW pairs (Figure 6). This means that the exponential growth rate is similar and does not depend on the MW of the polysaccharides. The existence of thicker films for the high-MW polysaccharides at a given bilayer number in the regime of steep growth is therefore not due to a larger incremental increase in the layer thickness per se,[20] but is rather attributable to an earlier crossover from the first to second phase of growth, as observed by AFM and confirmed by the a parameter value

(43) An apparently linear growth behavior was observed by radioactivity measurements for dried films consisting of HA modified with diethylenetriaminopentaacetic acid complexed with ^{111}In (see ref 15e). We are currently investigating the effect of polysaccharide modification on the film growth behavior.

(44) The crossover to an exponential growth regime is affected by the ionic strength of the deposition solutions. An exponential or quasi-exponential film growth has been reported for 0.01 M ≤ [NaCl] ≤ 0.15 M, while a linear increase in film thickness was observed for [NaCl] = 0.1 mM (see ref 20).

which is higher for the high-MW pair ($a = 8.2$) vs the low-MW construct ($a = 3.2$).

Both SPR and QCM data[20] show that exponential growth is a characteristic inherent to the HA/CH system. An exponential growth implies that there is a proportionality between the mass or thickness of the newly deposited HA/CH layer and the multilayer film thickness prior to the given deposition step.[8,20] Plots of the thickness of the (nth + 1) bilayer vs the thickness of the n-bilayer film obtained by SPR do in fact exhibit a linear tendency for all four bilayer pairs (Figure S5, Supporting Information). Both SPR and QCM results also reveal that the ultimate thickness of the multilayer, during the steep growth phase, depends critically on the size of the polysaccharides. Opposite trends emerge, however, from the data collected by the two techniques. QCM frequency shifts recorded for pairs consisting of HA of the same MW (400 000) and CH of different MWs (110 000−460 000) are such that it appears that the multilayers built with CH of lower MW are thicker than those constructed with CH of higher MW.[20] By contrast, Θ_m shifts generated from SPR scans acquired within the plasmon wave penetration depth reveal that the thicknesses of multilayers built with HA-360K/CH-160K and HA-31K/CH-160K are larger than those of multilayers of HA-360K/CH-30K and HA-31K/CH-30K, respectively (Figure 6). In other words, our data indicate that for a given MW of the nondiffusing HA, thicker films result from a higher molecular mass of the diffusing species CH. Likewise, we have found that for a given MW of CH, the higher MW HA gives thicker films.

For a given HA molecular weight, the concentration of uncompensated, fixed charges from polycation/polyanion pairs within the multilayer and net charge at the film/solution interface do not necessarily scale proportionally with the MW of CH used for multilayer buildup, due to the weak polyelectrolyte nature and charge mismatch of HA and CH. There is thus no reason to expect that the concentration of free polycation chains in the multilayer would increase proportionally when the CH molecular mass is decreased by a given factor, thereby resulting in films of equal or greater thickness (as suggested by the QCM frequency shifts),[20] provided that both the higher and lower MW CH can readily diffuse through the physical framework of the multilayer. The disagreement between the QCM and SPR results may in fact be only apparent. It is well-recognized that, for nonrigid films, a significant part of the QCM response is related to the viscoelastic properties of the coating.[29] QCM and SPR data may be reconciled if one assumes that the frequency shift monitored by QCM does not solely depend on the deposited mass, but is also influenced by the rheological properties of the multilayers.

The differences in growth pattern with polyelectrolyte molecular weight suggest the possible existence of a scaling law between the layer thickness and polyelectrolyte molecular weight. In fact, a plot of the multilayer thickness (reached after a specific number of deposited bilayers) as a function of the polysaccharide molecular weight yields a straight line, as exemplified in Figure S6 (Supporting Information) for data obtained after the deposition of 7, 7.5, and 8 bilayers. In this treatment, the MWs of the HA/CH complexes were taken as the average of the M_ns of their components. The scaling exponent obtained is 0.35 ± 0.06, a value similar to that reported by Shiratori and Rubner (~0.3) in a study of the weak polyelectrolyte pair, poly(acrylic acid)/poly(allylamine hydrochloride).[35]

Conclusions

We have explored the effect of the polysaccharide molecular weights on the growth and surface morphology of HA/CH multilayers constructed by the LbL technique onto PEI-primed gold surfaces. We show that the film thickness in the exponential growth phase depends on the molecular weights of the nondiffusing species HA and the diffusing species CH. That is, the higher the MWs of the polysaccharides, the thicker the multilayer for a given number of deposited bilayers. In the exponential growth phase, the film thicknesses decrease in the order HA-360K/CH-160K > HA-360K/CH-30K > HA-31K/CH-160K > HA-31K/CH-30K. Most importantly, exponential fits of the optical film thickness vs number of bilayers data yield similar values (~0.41−0.51) of the exponent b, which describes the film growth, indicating that the exponential growth rate is similar for all four MW pairs. Our combined SPR/AFM data strongly suggest that the polysaccharide MWs affect the onset of the steep (exponential) growth phase, and thereby the film thickness at a given stage, rather than the multilayer growth rate. This finding sheds new light into the exponential growth mechanism of polyelectrolyte layer-by-layer assemblies. To further investigate the role that the polyelectrolyte size plays on the buildup of HA/CH multilayers, additional measurements are in progress using polysaccharides spanning a wider range of MW, as well as techniques other than AFM and SPR (i.e. fluorescence spectroscopy and QCM).

Experimental Section

(A) Materials. Deionized water (resistivity, 18.2 MΩ cm) obtained by further purification of house-distilled water with a Milli-Q Gradient System (Millipore, Bedford, MA) was used for all the experiments. Sodium hyaluronan (HA-360K) was a gift from Hyal Pharmaceutical Corp. (Mississauga, ON) and HA-31K was received from Lifecore Biomedical (Chaska, Minnesota). Chitosans were purchased from Sigma Chemical Co. (CH-160K) and Wako Pure Chemicals (CH-30K). The degree of deacetylation of the chitosan samples was measured by ^{1}H NMR and UV−vis spectroscopy as described previously.[45] The characteristics of the polyelectrolytes are listed in Table 1. The HA and CH samples were used as received. Branched poly(ethyleneimine) (PEI; Aldrich, $M_w = 2.5 \times 10^4$ from light scattering, as stated by the supplier) was used without further purification. 11-Mercaptoundecanoic acid (MUA, 95%, Aldrich) was recrystallized twice from hexane prior to use.

(B) Polyelectrolyte Characterization. A GPC system consisting of an Agilent 1100 isocratic pump, a serial set of Shodex OH Pack SB-G and SP 806, 805, and 804 columns, a Dawn EOS multiangle laser light scattering detector (Wyatt Technology Corp.), and an Optilab DSP interferometric refractometer (Wyatt) was used to analyze the hyaluronan samples (injection volume, 100 μL; flow rate, 0.8 mL min^{-1}; eluent, aqueous 0.1 M $NaNO_3$/0.8 mM NaN_3). The chitosan samples were analyzed using a Viscogel GMPWxL column (injection volume, 100 μL; flow rate, 1.0 mL min^{-1}; eluent, aqueous 0.3 M CH_3COOH/0.3 M CH_3COONa/0.8 mM NaN_3). Their weight-average molecular weight and radius of gyration (R_g) were additionally checked by

(45) (a) Muzzarelli, R. A. A.; Rocchetti, R. In *Chitin in Nature and Technology*; Muzzarelli, R., Jeuniaux, C., Gooday, G. W., Eds.; Plenum Press: New York, 1985; pp 385−388. (b) Lavertu, M.; Xia, Z.; Serreqi, A. N.; Berrada, M.; Rodrigues, A.; Wang, D.; Buschmann, M. D.; Gupta, A. *J. Pharm. Biomed.* **2003**, *32*, 1149−1158.

multiangle laser light scattering using a CGS-3 goniometer (ALV GmbH) equipped with an ALV/LSE−5003 multiple-τ digital correlator, a He−Ne laser (632 nm), and a C25P circulating water bath (Thermo Haake). The molecular weight and radius of gyration (R_g) of each polymer were determined from the classical Zimm plots using the software supplied by the manufacturer. For light scattering experiments, the chitosans were dissolved in 0.3 M CH_3COOH/CH_3COONa solution.

(C) Polyelectrolyte Solutions. Solutions of 1.0 g/L polyelectrolyte concentration were used for multilayer film construction. These were prepared by direct dissolution of the polyelectrolytes in either aqueous 0.15 M NaCl (for PEI and HA) or aqueous 0.15 M NaCl/0.1 M CH_3COOH (for CH). The polyelectrolyte solution pH was adjusted to 4.5 (CH and HA) or 8.0 (PEI) using concentrated HCl or NaOH solutions. All polymer solutions were filtered through 0.45 μm Millipore PVDF filters prior to use.

(D) Surface Plasmon Resonance (SPR) Spectroscopy. (1) Apparatus. SPR spectroscopy makes use of resonant coupling between evanescent photons and surface plasmons to sense refractive index changes at a metal/liquid interface due to the adsorption or desorption of material.[31]

SPR measurements were carried out with a computer-controlled, scanning angle instrument (Resonant Probes GmbH, Goslar, Germany). Surface plasmons were excited at the metal/solution interface in the Kretschmann configuration using the p-polarized ouput from a HeNe laser (5 mW, 632.8 nm) and a right-angle LaSFN9 glass prism ($n = 1.845$, Hellma Optik). An optical chopper (Perkin-Elmer) was used to modulate the laser signal at a frequency of 1 kHz, which was then correlated with detection through the lock-in-amplifier. The light reflected from the metal/prism interface was focused onto a silicon photodiode detector. The photodiode signal was measured with a lock-in-amplifier (EG&G PAR) in-phase with the excitation source. A stepper-motor driven $\theta/2\theta$ goniometer (Huber) and motor control unit allowed the incident angle to be varied in increments $\geq 0.01°$. The goniometer and data acquisition were controlled through an IEEE interface board (Keithley model KPC-488.2) and software provided by Resonant Probes.

(2) In-Situ SPR Measurements. HA/CH multilayer film growth was monitored using both the angular reflectivity and kinetic modes. Angular reflectivity curves were obtained by measuring the reflected light intensity (R) as a function of the incident laser beam angle (Θ). The minimum of each curve corresponds to the resonance angle. Kinetic adsorption data (Θ_m-t) was obtained by tracking the angle of minimum reflectivity (Θ_m) over time (t) with a temporal resolution of 20 s. This was done by measuring the reflectivity at three points close to the overall reflectance minimum and fitting these to a parabola, the apex of which was taken as Θ_m. The shift in Θ_m is proportional to the amount of material adsorbed on the surface.[31]

(3) SPR Sample Cell and Substrate Preparation. A thin gold layer ($\sim$48 nm) was thermally evaporated onto LaSFN9 glass slides at a rate of $\sim$0.1 nm/s and base pressure of $\sim 1 \times 10^{-7}$ Torr using a VE-90 thermal evaporator equipped with a quartz crystal deposition monitor (Thermionics Vacuum Products, Port Townsend, WA). A self-assembled monolayer of MUA was prepared by incubating the gold-coated slides into a MUA solution in ethanol (1 mM) for at least 12 h. The backside of a MUA-functionalized Au substrate was optically coupled to the base of a LaSFN9 prism using a Cargille Series B liquid ($n = 1.700$). The prism/Au substrate assembly was then fixed against one side of a custom-built Teflon liquid cell (1 mL capacity) fitted with Kalrez O-rings so that the MUA−Au surface faced the inside of the cell. The other side of the liquid cell was pressed against a microscope glass slide. The prism/Au substrate/liquid cell assembly was mounted onto the goniometer stage so that the center of the Au/glass substrate was at the axis of rotation. The goniometer position at which the back-reflected beam overlapped with the incident beam was used to define the angle of incidence of 45° with an accuracy of $\pm 0.01°$.

(4) Multilayer Film Formation. Addition of buffer or polyelectrolyte solution into the SPR liquid cell was performed by manual injection. The deposition of polyelectrolyte was monitored under nonflow conditions. A primer layer of PEI was first deposited onto a MUA-modified gold surface by incubation of the substrate in an aqueous PEI solution (pH 8.0) inside the SPR cell for 30 min. The protonated PEI ($pK_a \approx 8.5$)[46] adsorbs onto the COO^- monolayer surface (reported pK_a values for a self-assembled MUA monolayer range from 5.5 to 7.5).[47] The cell was flushed with 10 mL (10× cell volume) of aqueous NaCl (0.15 M, pH 4.5) to ensure the removal of excess PEI and filled with aqueous NaCl. HA and CH were then alternately deposited on the PEI/MUA/Au surface, beginning with HA, by exposure to the polyelectrolyte solution for 20 min. The film surfaces were rinsed with 0.15 M NaCl (pH 4.5) solution between each HA or CH adsorption step. All experiments were done at room temperature.

Throughout the text, the term "layer" refers to a single polymer coating (HA or CH), while the term "bilayer" is used to describe the assembly of a pair of oppositely charged polyelectrolytes. The PEI/MUA/Au surface is defined as bilayer zero.

(5) Film Thickness Calculations. Using the Fresnel modeling software provided by Resonant Probes, angular reflectivity curves were analyzed with a five-layer model (glass prism/gold−MUA/PEI layer/HA-CH film/aqueous solution) to extract the total film thickness (d_{film}) following the alternate adsorption of each HA and CH layer. First, the critical angle position of the $R-\Theta$ scan for the MUA-modified Au film was fit, using the known dielectric constant of the LaSFN9 prism ($\epsilon = 3.404$), to obtain the dielectric constant of the 0.15 M NaCl (pH 4.5) solution ($\epsilon = 1.777$). Using this value for the dielectric constant of the NaCl solution, the entire $R-\Theta$ scan was then fit to obtain the complex dielectric constant, $-12.5 + 1.3i$ and thickness, 48.5 nm, for the MUA-modified Au film.

It is generally impossible to determine both ϵ_{film} and d_{film} for an adsorbed, thin organic film from a single SPR curve; any number of different combinations of ϵ_{film} and d_{film} can produce an angular reflectivity scan with the same Θ_{min} as the measured curve.[48] To obtain film thicknesses from $R-\Theta$ scans acquired within the range of the plasmon wave decay, the film dielectric constant must be known. Angular reflectivity scans recorded for sufficiently thick films consisting of more than 9 HA/CH bilayers (region of film growth where the resonance angles level off) were used to obtain values for ϵ_{HA} and ϵ_{CH}, and $\epsilon = 1.890$ was used for the PEI primer layer.

(E) Atomic Force Microscopy (AFM). (1) Imaging in Liquid. AFM imaging was performed in tapping mode with an extended Dimension 3100 scanning probe microscope and Nanoscope IIIa controller (Digital Instruments/Veeco). HA/CH multilayers were prepared directly in a custom-built, Teflon liquid cell as described above for the SPR measurements. To prevent any structural rearrangements of the film structure induced by jumps in the pH and/or ionic strength, each HA and CH deposition step was followed by a rinse with an aqueous NaCl solution of the same ionic strength (0.15 M) and pH (4.5) as the polyelectrolyte solutions, and all imaging was performed in the same NaCl solution.[49] Images were acquired at various stages of the buildup process. Surfaces were analyzed at the minimum applied force that would allow stable imaging using sharpened silicon nitride microlevers (model MSCT-AU, Veeco) with a typical radius of curvature of 20 nm, nominal spring constant of 0.1 N m^{-1}, and a resonance frequency of 7.55 kHz in liquid. The scan rate and image

(46) von Harpe, A.; Petersen, H.; Li, Y.; Kissel, T. *J. Control. Release* **2000**, *69*, 309−322.
(47) (a) Vezenov, D. V.; Noy, A.; Rozsnyai, L. F.; Lieber, C. M. *J. Am. Chem. Soc.* **1997**, *119*, 2006−2015. (b) Hu, K.; Bard, A. J. *Langmuir* **1997**, *13*, 5114.
(48) Chinowsky, T. M.; Yee, S. S. *Sens. Actuators, B* **1998**, *51*, 321−330.
(49) (a) Fery, A.; Scholer, B.; Cassagneau, T.; Caruso, F. *Langmuir* **2001**, *17*, 3779−3783. (b) Mendelsohn, J. D.; Barrett, J. C.; Chan, V. V.; Pal, A. J.; Mayes, A. M.; Rubner, M. F. *Langmuir* **2000**, *16*, 5017−5023. (c) Sukhorukov, G. B.; Schmitt, J., Decher, G. *Ber. Bunsen-Ges. Phys. Chem.* **1996**, *100*, 948−953.

resolution used are 1 Hz and 512 × 512 pixels, respectively. Several macroscopically separated areas of the multilayer films were examined, and representative height images are presented. The reported widths are those measured at half-height. Unless otherwise mentioned, root-mean-square surface roughness analyses were carried out on 7.5 μm × 7.5 μm scans using the Nanoscope software. Images used for RMS roughness analyses and film thickness measurements were corrected for bow/tilt by a third-order plane fit correction.

The surface morphology of the HA-360K/CH-160K and HA-31K/CH-30K multilayers remained stable in the NaCl solution during the 0.5−2 h period used to image and indent the films at each stage of buildup. In fact, 8 bilayer-thick films could be left overnight and imaged the following morning without any noticeable change in their surface morphologies.

(2) Film Thickness Measurements. While the HA/CH multilayers could be imaged nondestructively under fluid in tapping mode using appropriate parameters (drive amplitude of 1−1.2 V, setpoint corresponding to a tip oscillation damping of 25−35% of the free liquid amplitude, scan rate of 1 Hz), holes could be deliberately created in the films by repeatedly scanning a 9 μm^2 area under 0.15 M NaCl solution after lowering the setpoint to nearly its minimum value (drive amplitude of 1−1.2 V, tip oscillation damping of 75−85% of the free liquid amplitude) and increasing the scan speed to 20.3 Hz. The newly exposed area was then imaged by increasing the scan size to 225 μm^2 and returning to the normal imaging parameters. The appearance of the polycrystalline Au topography was taken as an indication that very little, if any, material was left in the hole. This procedure worked well for the PEI−(HA-31K/CH-30K)$_{12}$ film and for PEI−(HA-360K/CH-160K) up to 8 bilayers. Holes were created in the thicker PEI−(HA-360K/CH-160K)$_{12}$ film under 0.15 M solution in contact mode with a 0.32 N/m silicon nitride probe tip, 30 Hz scan rate, and setpoint amplitude of 9−10 V. Film thicknesses were determined by measuring the step heights between the bottom of the hole and the top film surface at several points along 8−12 different linear cross-sections.

Acknowledgment. This work was supported in part by a research grant of the Natural Sciences and Engineering Research Council of Canada (F.M.W.), an equipment grant of the Fonds québécois de la recherche sur la nature et les technologies (A.B. and F.M.W.), and the FQRNT Regroupement stratégique program (A.B. and F.M.W.).

Supporting Information Available: AFM topography images of PEI−MUA−Au substrate, PEI−(HA)$_1$, PEI−(HA/CH)$_7$−HA$_8$, PEI−(HA/CH)$_8$, PEI−(HA/CH)$_{10}$, and PEI−(HA/CH)$_{10}$−HA$_{11}$, the AFM image of an indented PEI−(HA-31K/CH-30K)$_{12}$ film, the plot of ϵ_{film} vs the number of deposited HA or CH layers, plots of the thickness of the (nth + 1) bilayer vs the thickness of the n-bilayer film obtained by SPR, and the dependence of the HA/CH multilayer thickness on the average molecular weight of the polysaccharides (PDF). This material is available free of charge via the Internet at http://pubs.acs.org.

JA044385N